

Title:

Evaluation of a novel elastic respiratory motion correction algorithm on quantification and image quality in abdomino-thoracic PET/CT

Authors:

Joseph G Meier¹, Carol C. Wu², Sonia L. Betancourt Cuellar², Mylene T. Truong², Jeremy J. Erasmus², Samuel A. Einstein¹, and Osama R. Mawlawi¹

¹Department of Imaging Physics, The University of Texas MD Anderson Cancer Center, Houston, TX

²Department of Diagnostic Radiology, The University of Texas MD Anderson Cancer Center, Houston, TX

Corresponding Author:

Osama R. Mawlawi

1515 Holcombe Blvd., Unit 1352, Houston, TX 77030

713-563-2711 (office) / 713-563-8842 (fax) / OMawlawi@mdanderson.org

First Author:

Joseph G Meier (Ph.D. Graduate Student)

1515 Holcombe Blvd., Unit 1352, Houston, TX 77030

713-422-3597 (cell) / 713-563-8842 (fax) / JGMeier@mdanderson.org

Manuscript Word Count: (4985)

Financial Disclosures: none

Short Running Title: Elastic motion correction in PET/CT

ABSTRACT

Our aim is to evaluate in phantom and patient studies a recently developed elastic motion deblurring (EMDB) technique which makes use of all the acquired PET data and compare its performance to other conventional techniques such as phase based gating (PBG) and HDChest (HDC) both of which use fractions of the acquired data. Comparisons were made with respect to static whole-body (SWB) images with no motion correction.

Methods: A phantom simulating respiratory motion of the thorax with lung lesions (5 spheres with ID=10- 28 mm) was scanned with 0, 1, 2, and 3 cm motion. Four reconstructions were performed: SWB, PBG, HDC, and EMDB. For PBG, the average (PBGave) and maximum bin (PBGmax) were used. To compare the reconstructions, the ratios of SUVmax (RSmax), SUVpeak (RSpeak), and CNR (RCNR) were calculated with respect to SWB. Additionally, 46 patients with lung or liver tumors < 3 cm diameter were also studied. Measurements of SUVmax, SUVpeak, and contrast-to-noise ratio (CNR) were made for 46 lung and 19 liver lesions. To evaluate image noise, the SUV standard deviation was measured in healthy lung and liver tissue and in the phantom background. Finally, subjective image quality of patient exams was scored on a 5 point scale by four radiologists.

Results: In the phantom, EMDB increased SUVmax/SUVpeak over SWB but to a lesser extent than the other reconstruction methodologies. The RCNR for EMDB however was higher than all other reconstructions (0.68 EMDB > 0.54 HDC > 0.41 PBGmax > 0.31 PBGave). Similar results were seen in patient studies. The SUVmax/SUVpeak were higher by 19.3/11.1% EMDB, 21.6/13.9% HDC, 22.8/12.8% PBGave, and 45.6/26.8% PBGmax compared to SWB. Lung/liver noise increased EMDB (3/15%), HDC (35/56%), PBGave (100/170%), and PBGmax (146/219%). CNR increased in lung/liver tumors only for EMDB (18/13%), and decreased for HDC (-14/-23%), PBGave (-39/-63%), and PBGmax (-18/-46%). Average radiologist scores of image quality were SWB (4.0 ± 0.8) > EMDB (3.7 ± 1.0) > HDC (3.1 ± 1.0) > PBG (1.5 ± 0.7).

Conclusion: The EMDB algorithm had the least increase in image noise, improved lesion CNR, and had the highest overall image quality score.

Key Words: Elastic Respiratory Motion Correction; PET/CT; noise reduction

INTRODUCTION

Static whole-body (SWB) PET acquisitions typically last 2-3 minutes per bed position, which can result in degraded PET image quality due to respiratory motion, particularly for tumors that are located in the lower thorax and upper abdomen (1-3). This potentially results in decreased measurements of activity concentration, overestimation of measured metabolic volume, and decreased lesion detectability, all of which could negatively affect patient management.

Many solutions exist to correct respiratory motion artifacts in PET/CT (4-10). However, all such methods first require the acquisition of the patient's respiratory waveform using external devices or data driven techniques. One of the first motion correction methods proposed was multi-bin respiratory gating (MBRG), which divides the acquired PET data into multiple bins corresponding to different respiratory phases or amplitudes of the breathing cycle. Fractioning the data into multiple bins increases the amount of noise per bin, however, which biases quantitative measures such as SUVmax and decreases image quality. These drawbacks can be overcome by longer acquisition time, but come at the expense of decreased patient comfort and reduced scanner throughput. Furthermore, while this approach allows the determination of the full range of tumor motion that is crucial for radiation therapy treatment planning it however increases the complexity of exam interpretation as it results in multiple image volumes corresponding to the different bins.

Another approach to reduce motion while avoiding the complexity of MBRG is end-expiration respiratory gating (EERG; 8,11). EERG is based on the observation that patients tend to spend more time in the end-expiration "quiescent" period of the breathing cycle, which corresponds to the least amount of motion (12). In comparison to an individual bin of MBRG, EERG has the advantage of using a larger fraction of the acquired PET data, resulting in less image noise while reducing motion blur, and creates only one PET volume for interpretation. EERG can be implemented using the amplitude or phase of the respiratory waveforms. In the phase-based approach, PET data corresponding to a preset phase offset and window width from the onset of each breathing cycle are retained. This approach is implemented commercially on GE PET/CT scanners as Q.Static (13). In the amplitude-based approach of EERG, implemented commercially as HDChest (HDC) on SIEMENS PET/CT scanners the user selects a percentage of the acquired PET data to preserve (8,14-16). The HDC algorithm analyzes the respiratory waveform to find the minimum amplitude range that contains the user-selected percentage of PET data, typically about 35%. EERG, whether phase- or amplitude- based has emerged

as the most common respiratory motion correction due to its simplicity and ease of use.

Elastic motion correction (EMC) is another approach for respiratory motion correction that retains all of the acquired PET data to create the final image. Using the entirety of PET data improves image quality, thereby reducing the acquisition times that are typical in respiratory motion-corrected exams. Two primary approaches exist for EMC. In one strategy, MBRG images are reconstructed, non-rigidly registered, and then averaged into a single volume (17). This approach has been implemented commercially by GE healthcare as Q.Freeze. A more recent approach (implemented commercially by SIEMENS and known as OncoFreeze) first derives a blurring kernel from sub-images (SWB and HDC) that are later used during image reconstruction to generate the final motion free image (18,19). To our knowledge there has been no independent evaluation of the EMDB algorithm with the exception of one small scale study (5 patients) presented as an abstract (20).

In this study, we evaluated these various respiratory motion correction methodologies (MBRG, ABOG, and EMDB) in comparison to SWB with no motion correction. Initially, a phantom evaluation was performed to provide a comparison of these algorithms with respect to the ground truth. We then assessed the impact of these various approaches on clinical PET lesion quantification as well as objective and subjective image quality. Numerous publications have studied the impact of MBRG and HDC, but, to the best of our knowledge, this is the first investigation that systematically evaluates the EMDB algorithm in comparison to other motion-correction techniques.

MATERIALS AND METHODS

Reconstruction Algorithms

In this study, four PET reconstructions were investigated. The first was SWB, which used all of the data with no respiratory motion correction. The second was MBRG, which reconstructed eight gates (each containing 12.5% of the PET data). The third was HDC which used the manufacturer-recommended 35% duty cycle for reconstruction. The fourth reconstruction was the EMDB algorithm (18,19), which used 100% of the acquired PET data to reconstruct a motion corrected image.

The EMDB algorithm initially performs an SWB reconstruction with 100% of the data, and an HDC reconstruction that applies a baseline shift-correction to the patient respiratory waveform. In this study, we

utilized a 35% duty cycle for the HDC image. The EMDB algorithm utilizes mass preservation optical flow(MPOF) (21) to non-rigidly register the reference volume (HDC) to the target volume (SWB) as seen in Figure 1. The HDC volume and the SWB volume have the same integral activity, but due to motion blur, the objects in each respective volume have different brightness, necessitating the MPOF algorithm to register the two volumes. MPOF does not require that the motion vectors correspond to physically realizable motion. EMDB uses MPOF to determine a fully 3D blurring kernel to redistribute the activity between the HDC SWB volumes. In the EMDB reconstruction, the blurring kernel is applied to the current image estimate before forward projection. The transpose of the blurring kernel, the deblurring kernel, is applied after back projection and results in a motion-corrected image estimate as seen in Figure 1.

Phantom Evaluation

A phantom was constructed to move five spheres in 3 dimensions to simulate the elastic motions of the abdomen and thorax. Detailed phantom description is provided in supplemental material. The spheres had inner diameters of 10, 13, 17, 22, and 28 mm. The spheres were placed in an acrylic tank containing 16 liters of water. and the spheres to background ratio was set to 5:1. . A motor drove the spheres using a repeated patient respiratory cycle that had a duration of 6 s. Four acquisitions were performed in which the spheres were driven with 0, 1, 2, and 3 cm amplitudes. The phantom motion was programmed such that the spheres always returned to the same location for all acquisitions. The phantom was scanned on a four-ring Siemens Biograph mCT Flow system (Siemens Healthineers; Erlangen, Germany), which has previously been characterized (22). CT-based attenuation correction (CTAC) data were acquired while the spheres were motionless, and at the initial position. The PET data were acquired during continuous bed motion (CBM) for 60 cm. In each acquisition, three table speed zones were prescribed: 1 mm/s for 15 cm superior to the acrylic tank, 0.5 mm/s for 30 cm covering the phantom tank and 1 mm/s for 15 cm inferior to the phantom tank. During PET acquisition, the respiratory waveform was acquired with the AZ-733V respiratory gating system (Anzai Medical Co., Ltd.; Tokyo, Japan) (23), by wrapping the belt around the surrogate motor platform (Figure 2). The phantom and setup are shown in Figure 2A and B and supplemental material. Each phantom scan was 15 minutes in duration. Care was taken to ensure that each acquisition had similar counting statistics, using list-mode rebinning of the acquired data. SWB, EMDB, HDC, and PBG reconstructions were performed for all phantom scans. All reconstructions were

performed with the default clinical parameters: 2 iterations, 21 subsets, time-of-flight information, point spread function correction, 200 x 200 matrix, 4.07 mm x 4.07 mm x 3mm voxel size, and 5 mm full-width at half-maximum isotropic Gaussian post-filtration.

For each motion amplitude and reconstruction algorithm, we measured SUVmax, SUVpeak, and SUV standard deviation (SD). SUVmax and SUVpeak were determined from a region of interest (ROI) encompassing each sphere. All measurements were made in MIM v6.6 (MIM Software, Inc.; Cleveland, OH). SUV SD was measured in the uniform background of the phantom with a 3-cm-diameter spherical ROI. Contrast to noise ratio (CNR) for each sphere was also calculated according to the Equation 1 using the sphere SUVmax (SUVmax,sp), background SUVmax (SUVmax,bg), and background SUV SD (σ).

$$CNR = \frac{SUV_{max,sp} - SUV_{max,bg}}{\sigma} \quad \text{Equation 1}$$

For each sphere, phantom scan, and reconstruction, the SUV and CNR ratio relative to the ground truth SWB reconstruction with no motion was calculated for SUVmax (RSmax), SUVpeak (RSpeak), and CNR (RCNR). For the measurements made on the eight gates of the PBG reconstruction, the average value of all eight gates was used (PBGave) as well as the gate with the highest value (PBGmax) for each respective measurement of SUVmax, SUVpeak, SUV SD, and CNR. The average SUV SD was calculated for all background spheres, phantom scans, and reconstruction algorithms.

Patient Evaluation

Forty-six patients (23 males and 23 females; mean age: 62.9 ± 14.8 ; mean BMI: 28.2 ± 6.7) with 65 lung (N=46) and/or liver (N=19) lesions located in regions impacted by respiratory motion and less than 3 cm in diameter were prospectively recruited for this study. The institutional review board (IRB) approved this study (MDACC IRB 2015-0989) and all subjects signed a written informed consent prior to imaging. Patients fasted for 6 hours before injection of 323 ± 56 MBq ^{18}F -FDG. The PET scan followed the FDG injection time by 69.2 ± 9.1 min.

PET/CT Acquisition and Image Reconstruction

All patients were scanned with the same PET/CT system and protocols as used for the phantom scans,

except that the patient PET data were acquired in CBM with 0.8-1 mm/s table speed, depending on patient BMI. Over the lung/liver region where tumor(s) were impacted by motion, a table speed of 0.5 mm/s was used for a 30 cm section of the scan. Patient respiratory waveforms were acquired with the Anzai system. All CT scans were acquired with free breathing. SWB, EMDB, HDC, and PGB reconstructions were performed for all patient scans, with the same reconstructions parameters as used for the phantom scans.

Image Analysis

The SUVmax and SUVpeak normalized by body weight were measured for each tumor. SUV SD (a surrogate for image noise) was measured using a 3-cm-diameter spherical ROI in lung and liver tissue that we assessed to be free of disease. The CNR was calculated analogous to Equation 1. All measurements were made in MIM 6.6. For the PBG reconstruction, both PGBave and PGBmax were analyzed.

Image Quality Assessment

Four radiologists experienced in PET/CT imaging subjectively scored the image quality of the four reconstructions on a Likert-type scale of 1 (poor) to 5(excellent). In total, 184 reconstructions (46 patients x 4 reconstructions) were assessed. For the PBG reconstructions, gate 5/8 was selected for presentation as this gate contained the least amount of motion. Only one reconstruction was displayed at a time for assessment. The order of the presentation was randomized by reconstruction method and patient. Only the images acquired from the 30 cm region scanned with 0.5 mm/s table speed were presented for image quality scoring. To assess intra-reader reliability, 20 cases were repeated.

Statistical Analysis

All statistical analyses were performed with R (v3.5.0 and irr package v0.84). Wilcoxon signed-rank tests, with Bonferroni corrections, were performed to determine significance. Krippendorff's alpha test (24) was used to assess inter- and intra-reader reliability in image quality assessment.

RESULTS

Phantom Evaluation

All motion correction methodologies successfully reduced image blur (Figure 2C). The average values of RS_{max} over all spheres and motion amplitudes were measured to be 0.85 (SWB), 0.96 (EMDB), 1.01 (HDC), 1.06 (PBG_{ave}), and 1.23 (PBG_{max}; Figure 3A). The average values of RS_{peak} were measured to be 0.87 (SWB), 0.94 (EMDB), 0.99 (HDC), 1.00 (PBG_{ave}), and 1.10 (PBG_{max}; Figure 3B). Only the SWB and EMDb reconstructions had decreasing RS_{max} and RS_{peak} with increasing sphere motion amplitude. The sphere with the smallest inner diameter (10 mm) had the largest decreases in RS_{max} and RS_{peak} as the motion amplitude increased. The percent increases in SUV SD compared to the SWB reconstruction were 24.6% (EMDB), 61.6% (HDC), 171.7% (PBG_{ave}), and 216.2% (PBG_{max}; Figure 3C). The average values of RCNR were 0.31 (PBG_{ave}), 0.41 (PBG_{max}), 0.54 (HDC), 0.68 (EMDB), and 0.74 (SWB; Figure 3D). Motion correction did not increase RCNR above the SWB value until the motion amplitude reached 3 cm and this was only for the EMDb and HDC reconstructions (Figure 3D). Decreases in RCNR relative to motion amplitude were only observed for the SWB and EMDb reconstructions (Figure 3D).

Patient Tumor Quantification

In comparison to the SWB reconstruction, all motion-correcting reconstruction algorithms displayed significant increases in SUV_{max} and SUV_{peak} (Figure 4A). The percent increases in SUV_{max} in comparison to SWB for EMDb, HDC, PBG_{ave}, and PBG_{max} were 19.3%, 21.6%, 22.8%, and 45.6%, respectively. The percent increases in SUV_{peak} in comparison to SWB for EMDb, HDC, PBG_{ave}, and PBG_{max} were 11.1%, 13.9%, 12.8%, and 26.8%, respectively. For measurements of both SUV_{max} and SUV_{peak}, PBG_{max} had the largest increase in comparison to SWB, while PBG_{ave}, HDC, and EMCBD had relatively similar increases with EMDb consistently having the lowest values. The percent increases in lung/liver SUV SD in comparison to SWB for EMDb, HDC, PBG_{ave}, and PBG_{max} were 3.3%/14.8%, 35.1%/55.8%, 100.0%/169.6%, and 145.8%/219.0%, respectively (Figure 4B) showing that EMDb consistently had the least increase in lung and liver SUV SD. Across all motion correction methodologies, the increases in the SUV SD, were higher in the liver in comparison to the lung. The percent increases for lung/liver lesion CNR in comparison to SWB for EMDb, HDC, PBG_{ave}, and PBG_{max} were 17.8%/13.3%, -13.9%/-23.2%, -38.6%/-62.7%, and -18.2%/-46.0%, respectively. EMDb was the only motion correction method that increased lesion CNR (other had negative results), although the increase in liver lesion CNR was not significant ($p=0.58$). Example patient images of all four reconstructions are shown in

Figure 5.

Subjective Image Quality

Out of the motion correction methods, the EMDB method was scored as having the best overall image quality (Figure 6). The percent changes in image quality in comparison to SWB for EMDB, HDC, and PBG were -9.7%, -22.6%, and -63.7%. The intra-reader repeatability alpha scores were 0.75, 0.77, 0.78, and 0.87. The inter-reader repeatability alpha score was 0.81.

DISCUSSION

We assessed the impact of various motion correction methodologies on PET/CT imaging, with a primary interest in evaluating the EMDB technique. This is the first published study on the impact of the EMDB algorithm in comparison with other motion correction methodologies on a relatively large cohort of patients.

The most important finding of this investigation was that the EMDB algorithm had the smallest increase in image noise while reducing motion blur and improving lesion contrast. The primary cause of the reduced image noise was that the algorithm used all of the acquired PET data as opposed to the other motion correction methodologies, which used smaller fractions of the data. These findings were consistent for both phantom and patient studies and were corroborated by the objective physician evaluation.

Although the EMDB algorithm used all of the acquired PET data in the reconstruction, the resultant images still had higher noise when compared to SWB. We postulate that this noise resulted from the determination of the blurring kernel between the noisy HDC image and the SWB image in the EMDB algorithm. Specifically, the blurring kernel is influenced by the noise in the HDC image. In this regard, the choice of the percent duty cycle for the HDC image has a very important consequence on EMDB image quality. Increasing the duty cycle would reduce noise, but at the expense of increased image blur, while decreasing the duty cycle has the opposite effect.

Several investigators have previously shown that image blur is reduced when using PET data corresponding to only a small fraction of the breathing cycle (25,26). However, one significant consideration when implementing such motion correction approaches are the artifactual increases in measured SUVmax and SUVpeak due to increased image noise. As seen in our phantom and patient results, SUVmax and SUVpeak

increased for all motion correction methodologies. However, these increases were amplified with decreasing amount of PET data. Our phantom results indicate that image noise increased with methods that use decreasing amounts of PET data (increasing from 24.6% for EMDB to 216.2% for the PBGmax approach). In this regard, an increase in SUVmax or SUVpeak when using such correction techniques should not only be attributed to motion correction but rather also to an increase in image noise. In this work we used CNR as a metric to capture both of these image attributes (SUVmax and noise), and the results clearly show a decrease in CNR with correction methodologies that use decreasing amounts of PET data (figure 3D) reflecting the larger increase in image noise compared to a true increase in SUVmax.

One important finding about the EMDB algorithm is its degraded performance with increasing motion amplitude. Our results indicate that while all other motion correction methodologies resulted in SUVmax/SUVpeak that were relatively independent of motion amplitude, the EMDB algorithm decreased these values with increasing motion but to a lower extent than SWB (Figure 3 A and B). It is not clear why this performance was observed but further investigation is warranted.

In patient data, the percent increases in SUVmax and SUVpeak were very similar for EMDB, HDC, and PBGave. PBGmax, however, had the highest percent increases. The large differences seen between measured SUV for PBGmax compared to the other motion corrections methodologies is attributed to increases in image noise. EMDB had the least amount of noise increase, yet the increases in SUVmax and SUVpeak are similar in comparison to HDC and PBGave, which use much less of the data. From this, we can infer that the increases in SUV for the EMDB algorithm were influenced more by reductions in motion blur and less by increases due to noise bias.

Our results show that EMDB was the only method that improved CNR, although not significantly for liver lesions primarily due to the relatively high noise in the liver that neutralized any increased in liver SUV. Overall however, EMDB increased measured SUVmax and SUVpeak yet had the least increase in image noise and, as a result, was the only method to improve lesion CNR. Although SUVmax and SUVpeak increased for the other motion correction methodologies, all of them decreased the CNR of the lesions.

Our image quality scores confirmed our expectations of low scores with increased image noise. Of the motion correction methodologies, the EMDB algorithm had the highest overall score, presumably because it contained the least amount of image noise. The SWB images incurred substantial respiratory motion blur in

comparison to the motion correction methodologies, however, the image quality scores show that the primary concern in overall image quality was the amount of image noise that was present. In addition, our assessment of our inter-reader reliability showed good agreement between readers. A meta-analysis of the physician scores showed that in 50% of the cases, the physicians scored the EMBD images with similar or better quality than the SWB images. This number was 25% for cases in which the physicians scored the EMBD as strictly better than the SWB images. These results suggest that physicians either preferred images with reduced blur or could not perceive changes in background noise between these two reconstruction algorithms.

One limitation of this study was that patient CTAC data were acquired under free-breathing conditions. The literature has shown that mismatches in free breathing CT and PET data often occur in areas impacted by respiratory motion and can impact SUV quantification (27,28). It is possible that the quantification results of this study were affected by these attenuation correction mismatches. Recent work in collaboration with our group has investigated the effects of these mismatches and have developed approaches to mitigate them (29). However, it would be interesting to assess the effect of such mismatch specifically on the performance of the EMBD algorithm as compared to other techniques.

Another limitation of this study is that all motion correction methods with the exception of the EMBD were performed without baseline shift correction of the respiratory waveform. (The EMBD algorithm had this feature imbedded in the software). In some patients, however, there can be a baseline drift in the respiratory waveform throughout the course of the examination that could affect the results of the various correction methods. In this regard, this data processing difference might have biased the results in favor of the EMBD algorithm. Analysis of the results with baseline shift for all the other correction methods will be a focus of future investigations.

CONCLUSION

All methods of motion correction reduced image blur but increased image noise, resulting in increased measurements of SUV. The EMBD algorithm had the least amount of noise increase, which resulted in improved CNR and higher image quality scores.

DISCLOSURES

The authors have no financial conflicts of interest related to the material presented in this article.

ACKNOWLEDGMENTS

The authors acknowledge the support of Siemens Medical Solutions USA Inc. for providing the EMDb software under a research agreement. We also acknowledge the support of Drs. James Hamill, Judson Jones, and Inki Hong from Siemens for their technical support. Special thanks to Drs. Lawrence Court and Arvid Rao at MD Anderson Cancer Center for providing the dynamic thorax phantom and advisement on statistical analysis respectively.

REFERENCES

1. Nehmeh SA, Erdi YE, Ling CC, et al. Effect of respiratory gating on reducing lung motion artifacts in PET imaging of lung cancer. *Med Phys*. 2002;29:366-371.
2. Froud R, McDermott G, Scarsbrook A. Respiratory-gated PET/CT for pulmonary lesion characterisation—promises and problems. *Br J Radiol*. 2018;91:1-9.
3. Crivellaro C, De Ponti E, Elisei F, et al. Added diagnostic value of respiratory-gated 4D 18F–FDG PET/CT in the detection of liver lesions: a multicenter study. *Eur J Nucl Med Mol Imaging*. 2018;45:102-109.
4. Nehmeh SA, Erdi YE, Meirelles GSP, et al. Deep-inspiration breath-hold PET/CT of the thorax. *J Nucl Med*. 2007;48:22-26.
5. Dawood M, Büther F, Lang N, Schober O, Schäfers KP. Respiratory gating in positron emission tomography: A quantitative comparison of different gating schemes. *Med Phys*. 2007;34:3067-3076.
6. Qiao F, Clark JW, Pan T, Mawlawi O. Joint model of motion and anatomy for PET image reconstruction. *Med Phys*. 2007;34:4626-4639.
7. Chang G, Chang T, Pan T, Clark JW, Mawlawi OR. Joint correction of respiratory motion artifact and partial volume effect in lung/thoracic PET/CT imaging. *Med Phys*. 2010;37:6221-6232.
8. van Elmpt W, Hamill J, Jones J, De Ruyscher D, Lambin P, Öllers M. Optimal gating compared to 3D and 4D PET reconstruction for characterization of lung tumours. *Eur J Nucl Med Mol Imaging*. 2011;38:843-855.
9. Nehmeh SA. Respiratory Motion Correction Strategies in Thoracic PET-CT Imaging. *PET Clin*. 2013;8:29-36.
10. Kesner AL, Meier JG, Burckhardt DD, Schwartz J, Lynch DA. Data-driven optimal binning for respiratory motion management in PET. *Med Phys*. 2018;45:277-286.
11. Frey K, Hamill J, Jones J, Koeppe R. Respiratory motion gated PET with end-expiratory, amplitude based gating [abstract]. *J Nucl Med* . 2009;50(suppl 2):348.
12. Liu C, Pierce II LA, Alessio AM, Kinahan PE. The impact of respiratory motion on tumor quantification and delineation in static PET/CT imaging. *Phys Med Biol*. 2009;54:7345-7362.

13. Hope TA, Verdin EF, Bergsland EK, Ohliger MA, Corvera CU, Nakakura EK. Correcting for respiratory motion in liver PET/MRI: preliminary evaluation of the utility of bellows and navigated hepatobiliary phase imaging. *EJNMMI Phys.* 2015;2:1-11.
14. Van Der Gucht A, Serrano B, Hugonnet F, Paulmier B, Garnier N, Faraggi M. Impact of a new respiratory amplitude-based gating technique in evaluation of upper abdominal PET lesions. *Eur J Radiol.* 2014;83:509-515.
15. Grootjans W, de Geus-Oei L-F, Troost EGC, Visser EP, Oyen WJG, Bussink J. PET in the management of locally advanced and metastatic NSCLC. *Nat Rev Clin Oncol.* 2015;12:395-407.
16. Hamill J, Ghosh P. HD•Chest Respiratory Gating for PET. In: PN0002262 Rev. A (White Paper). Siemens Medical Solutions; 2011.

[https://www.healthcare.siemens.com/siemens_hwem-hwem_sxxa_websites-context-](https://www.healthcare.siemens.com/siemens_hwem-hwem_sxxa_websites-context-root/wcm/idc/groups/public/@global/@imaging/@molecular/documents/download/mdax/ntk5/~edisp/whitepaper01_hd.chest.2-00838487.pdf)

[root/wcm/idc/groups/public/@global/@imaging/@molecular/documents/download/mdax/ntk5/~edisp/whitepaper01_hd.chest.2-00838487.pdf](https://www.healthcare.siemens.com/siemens_hwem-hwem_sxxa_websites-context-root/wcm/idc/groups/public/@global/@imaging/@molecular/documents/download/mdax/ntk5/~edisp/whitepaper01_hd.chest.2-00838487.pdf)17. Dawood M, Buther F, Xiaoyi Jiang, Schafers KP.

Respiratory Motion Correction in 3-D PET Data With Advanced Optical Flow Algorithms. *IEEE Trans Med Imaging.* 2008;27:1164-1175.

18. Hong I, Jones J, Casey M. Ultrafast Elastic Motion Correction via Motion Deblurring. In: 2014 IEEE Nuclear Science Symposium and Medical Imaging Conference (NSS/MIC). IEEE; 2014:1-2.
19. Hong I, Jones J, Hamill J, Michel C, Casey M. Elastic motion correction for continuous bed motion whole-body PET/CT. In: 2016 IEEE Nuclear Science Symposium, Medical Imaging Conference and Room-Temperature Semiconductor Detector Workshop (NSS/MIC/RTSD). IEEE; 2016:1-2.
20. Poesse S, Hong I, Mannweiler D, et al. Respiratory motion compensation in PET/CT: Evaluation of a fast elastic motion compensation technique based on motion deblurring [abstract]. *J Nucl Med.* 2017;58(suppl 1):1349.
21. Dawood M, Gigengack F, Jiang X, Schäfers KP. A mass conservation-based optical flow method for cardiac motion correction in 3D-PET. *Med Phys.* 2013;40:1-9.
22. Rausch I, Cal-González J, Dapra D, et al. Performance evaluation of the Biograph mCT Flow PET/CT system according to the NEMA NU2-2012 standard. *EJNMMI Phys.* 2015;2:1-17.
23. Li XA, Stepaniak C, Gore E. Technical and dosimetric aspects of respiratory gating using a pressure-

- sensor motion monitoring system. *Med Phys*. 2005;33:145-154.
24. Krippendorff K. Reliability in Content Analysis. *Hum Commun Res*. 2004;30:411-433.
 25. Bettinardi V, Rapisarda E, Gilardi MC. Number of partitions (gates) needed to obtain motion-free images in a respiratory gated 4D-PET/CT study as a function of the lesion size and motion displacement. *Med Phys*. 2009;36:5547-5558.
 26. Liu C, Alessio A, Pierce L, et al. Quiescent period respiratory gating for PET/CT. *Med Phys*. 2010;37:5037-5043.
 27. Pan T, Mawlawi O, Nehmeh SA, et al. Attenuation Correction of PET Images with Respiration-Averaged CT Images in PET/CT. *J Nucl Med*. 2005;46:1481-1487.
 28. Erdi YE, Nehmeh SA, Pan T, et al. The CT Motion Quantitation of Lung Lesions and Its Impact on PET-Measured SUVs. *J Nucl Med*. 2004;45:1287-1292.
 29. Hamill J, Mawlawi O, Meier J. Respiratory Phase Matching in PET/CT Using Fast Spiral CT [abstract]. *J Nucl Med*. 2017;58(suppl 1):577.

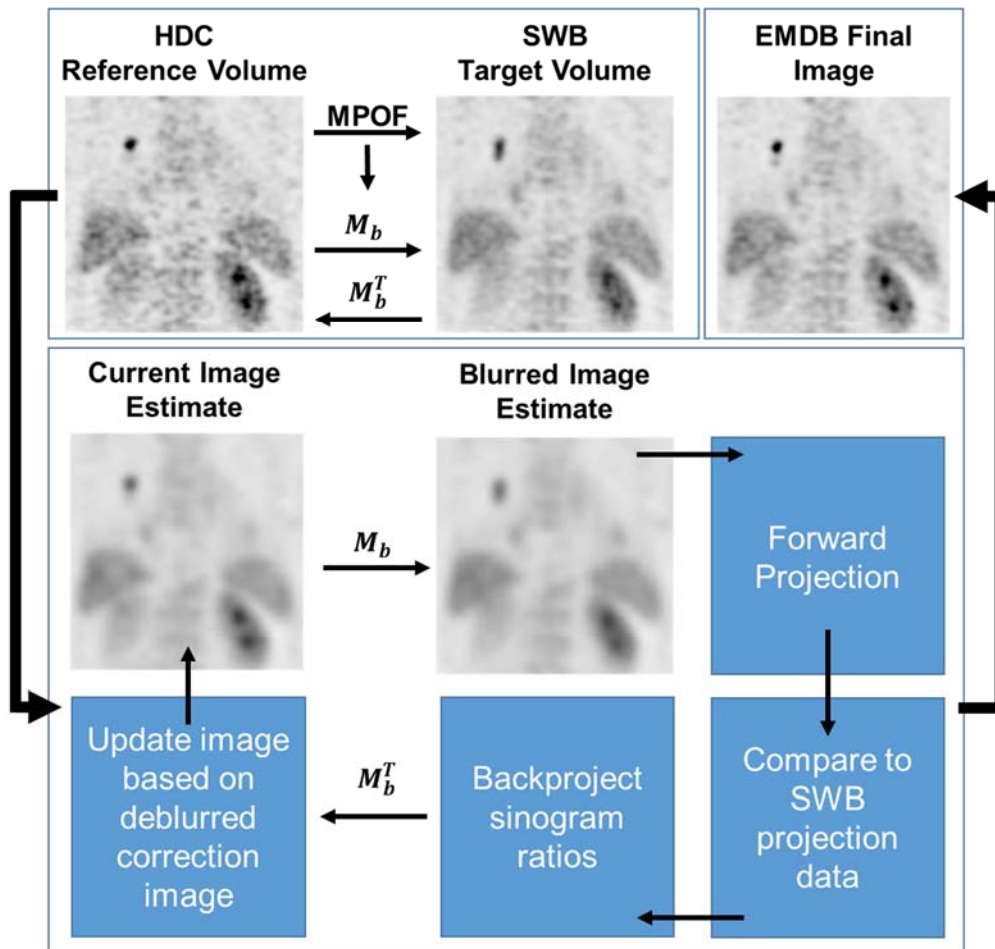


Figure 1: Workflow of the EMD algorithm.

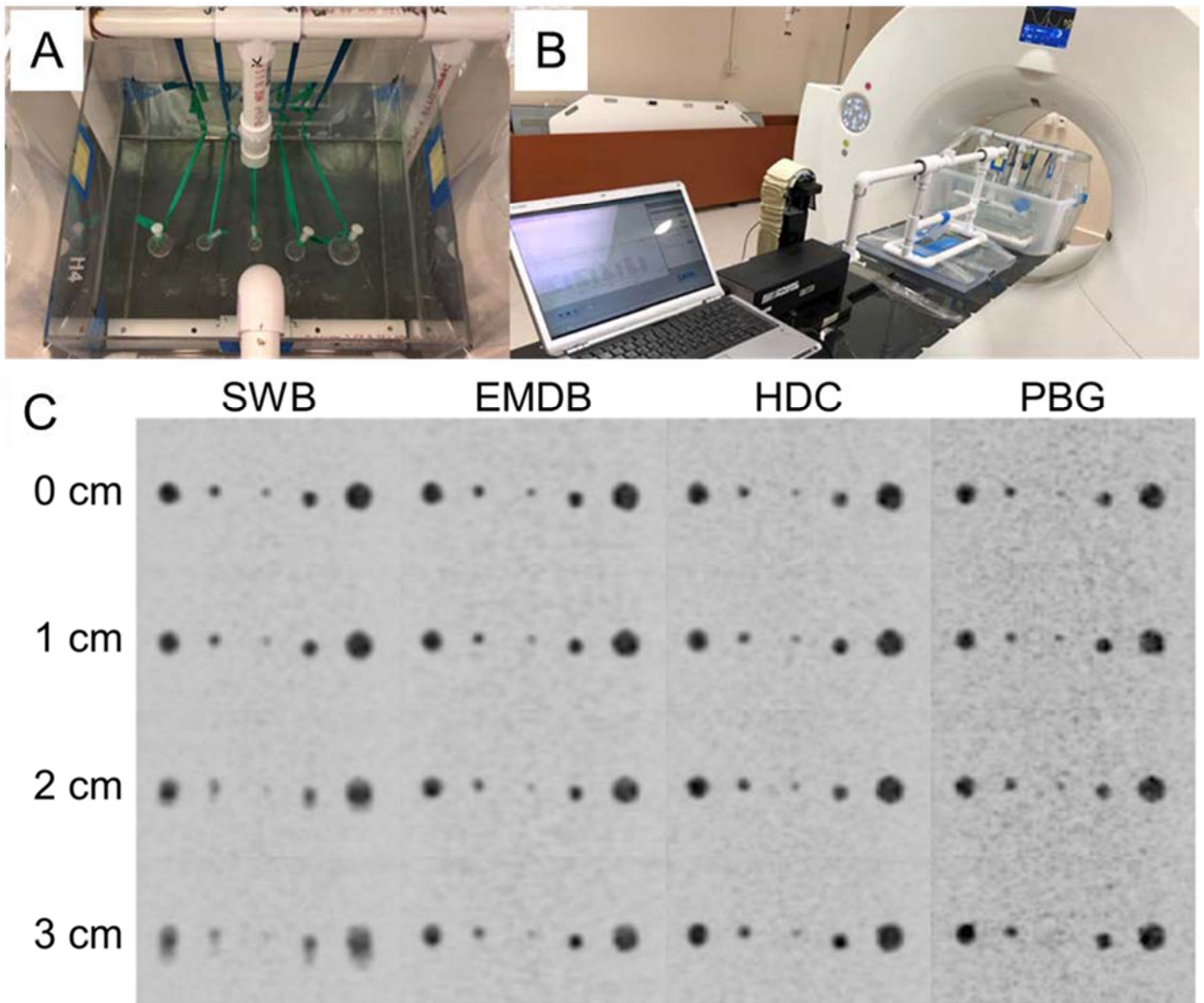


Figure 2: Phantom experimental setup and results. A) Acrylic tank and spheres. B) Spheres driven in the superior-inferior direction by dynamic thorax phantom motor (right). C) MIP images of phantom for the four phantom acquisitions with varying motion and 4 reconstruction methods: static whole body (SWB; no motion correction), elastic motion correction via deblurring (EMDB), HDChest (HDC), and phase-based gating (PBG; 1/8 gates).

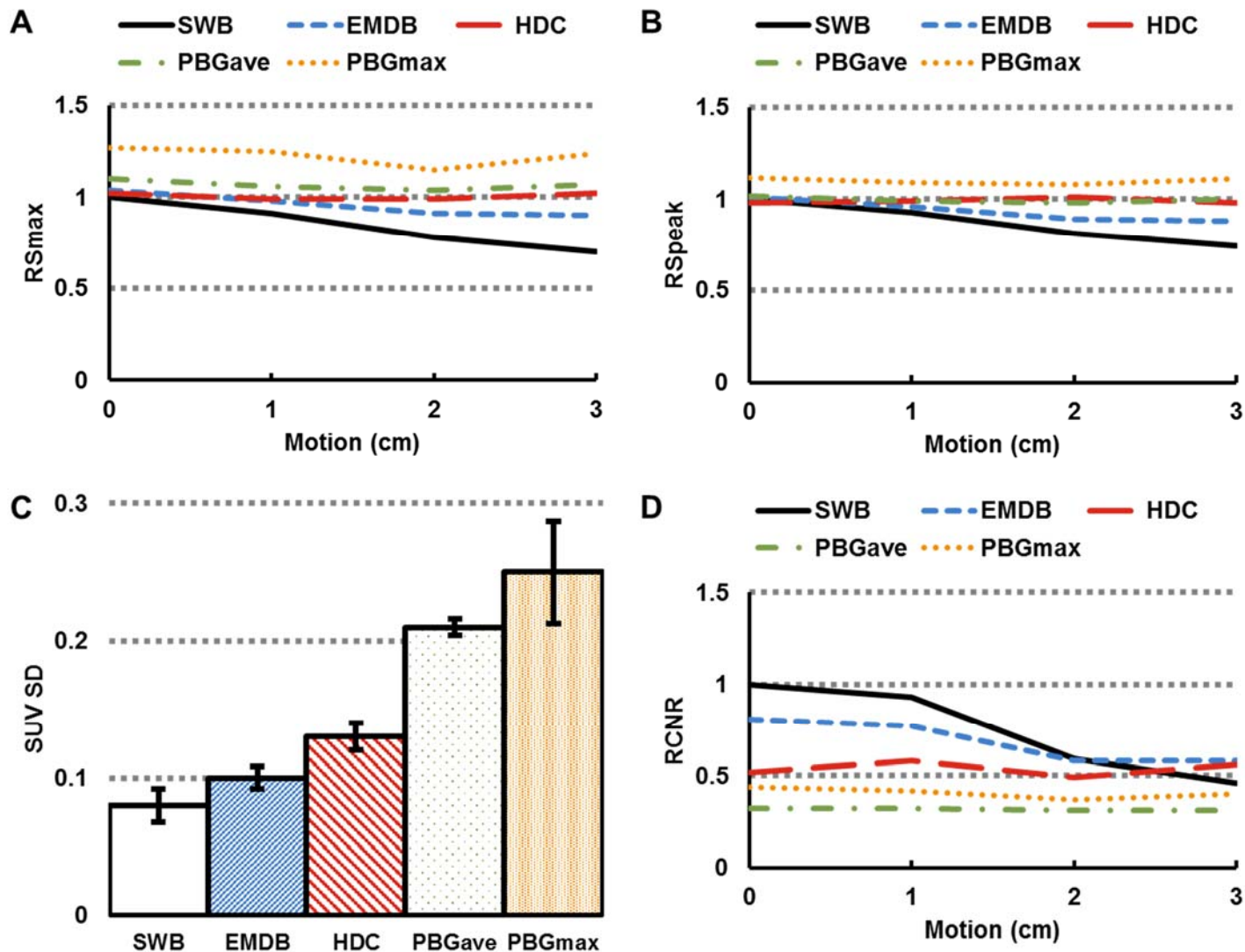


Figure 3: Phantom experimental measurements. A) SUVmax normalized to SWB (RSmax) and B) SUVpeak normalized to SWB (RSpeak) variation due to sphere displacement. C) SUV standard deviation (SD) in background across all reconstructions. D) Contrast-to-noise ratio normalized to SWB (RCNR) variation due to sphere displacement. The values shown are for the average of all spheres.

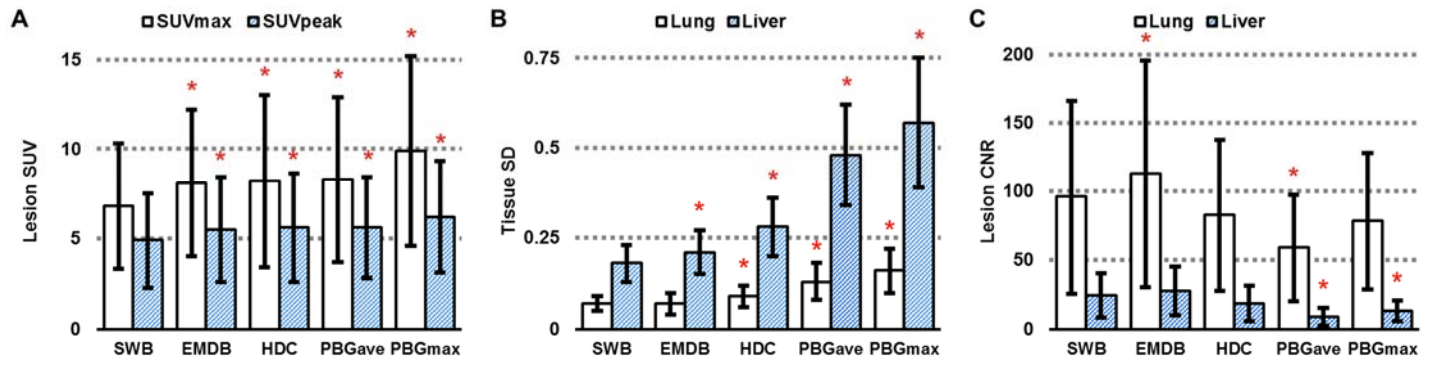


Figure 4: Measured A) SUVmax and SUVpeak for 65 lesions, B) lung and liver SUV standard deviation (SD), and (C) lung and liver lesion contrast-to-noise ratios (CNR). Significant differences ($p < 0.01$) are indicated by *.

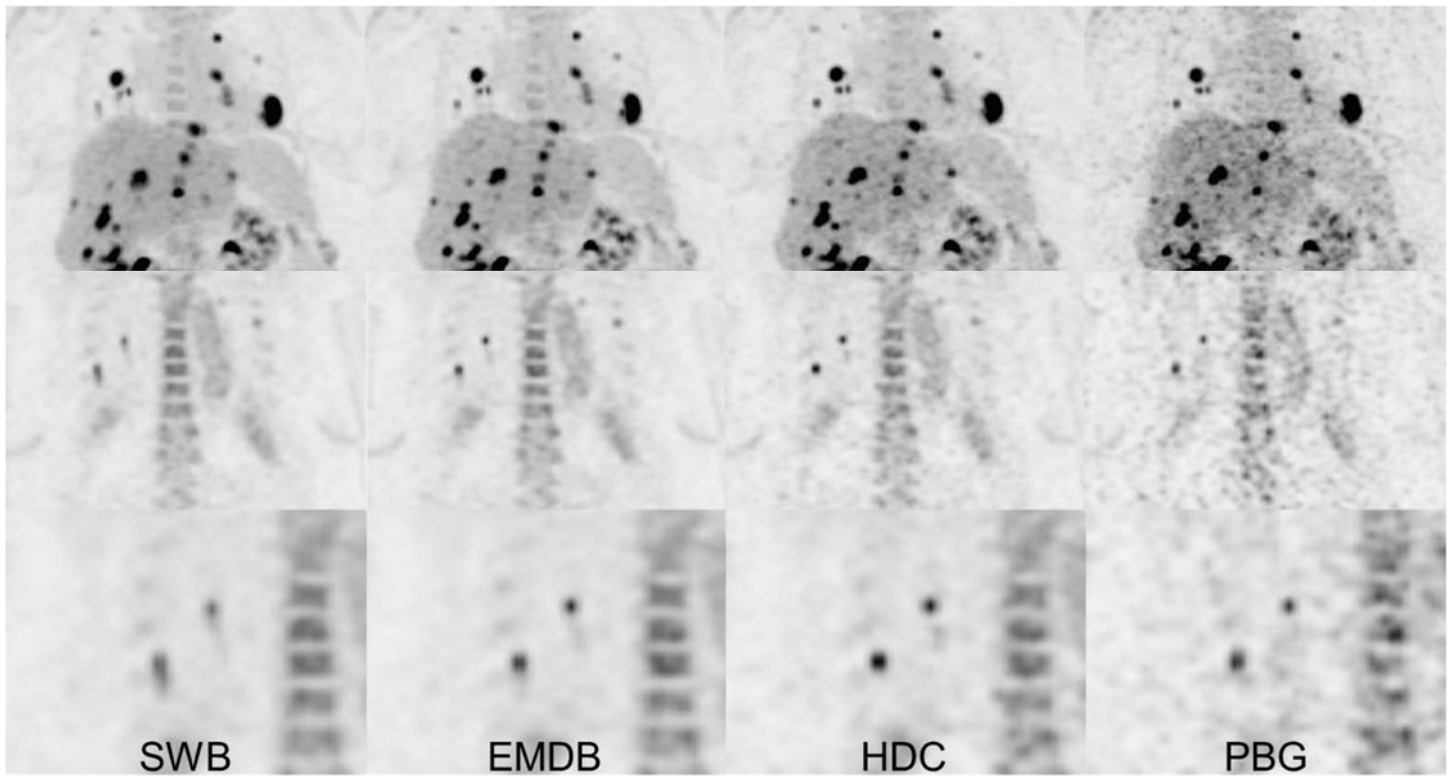


Figure 5: Example patient images. Top row: MIP images of all reconstructions. Middle row: Coronal plane view of right lung tumors. Bottom row: Zoomed view of the middle row.

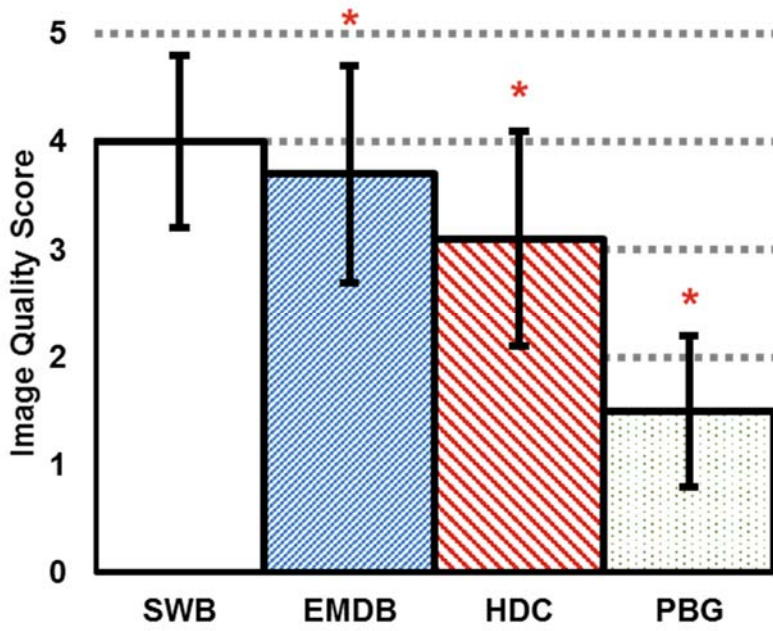
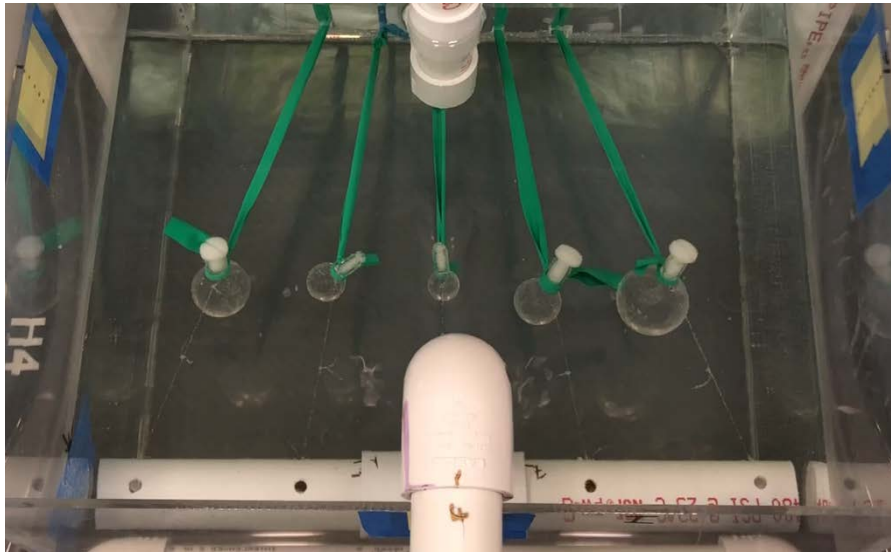


Figure 6: Mean value of the image quality score for the different reconstructions. Error bars represent one standard deviation. Significant differences ($p < 0.01$) are indicated by *.

Supplemental Material

The phantom was designed to move 5 spheres in three planes to simulate the elastic motions of the thorax and abdomen. To achieve this 3D motion, the CIRS dynamic thorax phantom (Norfolk, Virginia) motor moved the shaft of the phantom in the superior inferior direction as shown in the figure below [Also figure 2 in the manuscript]).



To simulate the anterior posterior motion of lung tumors, the stationary, superior attachment point of the spheres was placed at a depth of 11 cm, and the inferior mobile connection point of the spheres was placed at 6 cm, so that the depth of the spheres changed as the phantom moved. Furthermore, the attachment points of the spheres were spaced with less distance on the superior, stationary attachment point, in comparison to the inferior attachment point, such that the spheres paths diverged with inhalation, and converged with exhalation. The connection to the spheres from the superior location was made with elastic bands, while the connection to the mobile inferior shaft was non-elastic. Please refer to the movie below to see the sphere motion trajectory.



IMG_1614.mp4

The spheres had inner diameters of 10, 13, 17, 22, and 28 mm. The spheres were placed in an acrylic tank containing 16 liters of water. The spheres to background ratio was set to 5:1. . A motor drove the spheres using a repeated patient respiratory cycle that had a duration of 6 s. Four acquisitions were performed in which the spheres were driven with 0, 1, 2, and 3 cm amplitudes. The phantom motion was programmed such that the spheres always returned to the same location for all acquisitions. During PET acquisition, the respiratory waveform was acquired with the AZ-733V respiratory gating system (Anzai Medical Co., Ltd.; Tokyo, Japan), by wrapping the belt around the surrogate motor platform as shown by the red arrow in the figure below [Also figure 2 in the manuscript].

